CrossMark

The Influence of ScF$_3$ Nanoparticles on the Physical and Mechanical Properties of New Metal Matrix Composites Based on A356 Aluminum Alloy

S. VOROZHTSOV,[1,2,3] I. ZHUKOV,[1] V. PROMAKHOV,[1] E. NAYDENKIN,[1,2] A. KHRUSTALYOV,[1] and A. VOROZHTSOV[1]

1.—National Research Tomsk State University, Tomsk, Russia 634050. 2.—Institute of Strength Physics and Materials Sciences SB RAS, Tomsk, Russia 634055. 3.—e-mail: vorn1985@gmail.com

The development of the aerospace and automotive industries demands the development of aluminum alloys and composites reinforced with new nanoparticles. In this work, metal matrix composites (MMC) with an A356 aluminum alloy matrix reinforced with 0.2 wt.% and 1 wt.% of ScF$_3$ nanoparticles were produced by ultrasonic dispersion of nanoparticles in the melt followed by casting in a metallic mold. Structure as well as physical and mechanical properties of the cast samples were examined using electron and optical microscopy, hardness and tensile testing. It is shown that nanoparticles clusters are formed during the solidification at grain boundaries and silicon inclusions. Increasing nanoparticles content significantly reduced the grain size in the MMC and increased the mechanical properties—ultimate tensile strength, elongation and hardness. The contribution of different strengthening mechanisms is discussed. It is suggested that the coefficient of thermal expansion mismatch between the nanoparticles ScF$_3$ and the aluminum matrix is a dominant strengthening mechanism.

INTRODUCTION

Metal matrix composites (MMC) based on aluminum reinforced with different nanoparticles are nowadays of great interest in various fields of technology due to their good strength-to-weight ratio, high hardness, durability, etc.[1–4] The application of these composites is expected to expand and, therefore, a large amount of by-products and waste will be generated from the manufacturing process in the near future.

Casting is considered as a very popular method due to its unique features. In this method, the reinforcing particles are mixed into the metal melt and thoroughly distributed under stirring (or another external field) for a homogeneous mixture with the matrix alloy.

An A356 aluminum alloy[5] due to excellent castability, good weldability, excellent corrosion resistance, wear resistance properties, environmental friendliness and mechanical properties has a wide range of applications including automotive and aerospace industry.[6–8] Micro- and nanosized particles of metals and their compounds can be used as reinforcing particles.[1–4,8–10] Particle reinforcement blocks dislocation and grain boundary motion and effectively strengthens the material at room and high temperatures. In this case, the reinforcement effect is determined by three main factors: particle size, their volumetric concentration and spatial distribution. High efficiency of using high-modulus thermally stable compounds particularly oxides and carbides of the metals has been pointed out in a number of works.[3,10–13] In the case of optimal reinforcement loading and distribution, the following can be achieved for light alloys: wider working temperature range, significant improvement of strength, Young's modulus, and wear resistance, and reduced thermal expansion. However, in the majority of cases, particles with an average size of up to 10 μm are used with a considerable loading of 5–20%.[14–16] There is a good reason to believe[1,4,6–8,11] that the reduction of the average particle size to several tens of nanometers will make it possible to enhance the properties of Al-based MMCs at a much lower loading.

It is well known that the direct introduction of non-metallic particles (especially nanosized ones) into liquid metal is very challenging due to the fact that they are prone to agglomeration and flotation caused by their poor wettability by the liquid metal.[3,8,17] This problem can be solved using the impact of external fields on the metallic melt. External fields (e.g., ultrasonic cavitation) can facilitate wetting of the particles, breaking down the particle agglomerates and homogeneous distribution of the particles throughout the melt volume and, eventually, throughout the billet structure.[18]

In this paper, we combine previous expertise with the introduction of a principally new type of particles, i.e. ScF_3, which feature a negative coefficient of thermal expansion (NTE), into the Al-alloy matrix. The stability of the ScF_3 compound provides a higher melting temperature (1550°C) than the melt temperature processing of the composite (760°C). Radial compression and tensile tangential stresses around the particles form due to the fact that thermal expansion of reinforcing particles is lower than the thermal expansion of the matrix which may create an additional reinforcing effect.

MATERIALS AND METHODS

Preparation of Preformed Mixture Containing ScF_3 Nanoparticles

ScF_3 nanoparticles ($\sim$60 nm) synthesized using sol–gel technology[19] was selected for reinforcement. Aluminum powder ($\sim$20 μm) was used as the matrix material for making preformed mixtures. In order to improve the introduction of particles into the melt, nanopowder ScF_3 was premixed with the Al powder in an ultrasonic bath for 10 min in petroleum ether (99 wt.%) with additional 1 wt.% of stearic acid as a surface-active substance. ScF_3 nanoparticle content in the powder mixture with the aluminum was 20 wt.%. Then, the powder mixture was wrapped in aluminum foil. In fact, these rods can be considered as master alloys, but not as dense as described in Ref. 3.

Production of Aluminum-Based Metal Matrix Composites

An aluminum alloy A356 was melted in a graphite crucible with a total melt volume of 700 g. The ultrasonic processing was performed using a 5-kW water-cooled magnetostrictive transducer with a working frequency of 17.1 kHz and with a Nb sonotrode. First, ultrasonic degassing was performed at a melt temperature of 760°C for 1 min. Then, the preformed mixture Al-20 wt.% ScF_3 was introduced into the ultrasonic cavitation zone in the melt, directly under the sonotrode. After the introduction of the preformed mixture, the melt was treated with ultrasound for another 2 min at 720–740°C. Then, the obtained mixture was poured at 710°C into a metallic mold with the cavity size of

dia. 30 mm$\times$ 200 mm. The nominal nanoparticles content sin the alloy were 0.2 wt.% and 1 wt.%. A reference sample was produced using the similar processing parameters but without the introduction of the preformed mixture with nanoparticles ScF_3.

Methods of Structure and Properties Investigation

The ScF_3 powder was characterized using a JEM 2100 transmission electron microscope (TEM). The particle size in powders was calculated using Mastersizer 2000 particle size analyzer and the value of specific surface area of the powder was calculated from the average particle size using the Brunauer–Emmett–Teller (BET) method. The phase composition of the initial powders and the MMCs obtained was determined in an x-ray diffraction (XRD) Shimadzu 6000 x-ray diffractometer with CuKa radiation.

The structures of the obtained materials were studied by scanning electron microscopy (SEM) in a Philips SEM 515 microscope, as well as by optical microscopy (Olympus GX71). The polished alloy surface was anodized in order to study the microstructure of the obtained alloys. This procedure was performed using a 5% HBF_4 solution as an electrolyte at a voltage of $\sim$20 VDC.

Flat tensile samples 1 mm thick with a gauge length of 40 mm were cut from cylindrical castings and tested in a tensile machine Instron 3369 at a strain rate of 2×10^{-4}/s. Three samples were tested for each condition. Microhardness was measured using Nano Indenter G200/XP tester with a load of 250 g. At least three samples were tested for each condition and the average data are reported.

RESULTS AND DISCUSSION

Nanopowder ScF_3

A typical image of particles in the powder is shown in Fig. 1a. The BET surface area is equal to 17 m^2/g. Based on the specific surface area of the powder, the total pore volume in the agglomerates was calculated as 0.28 cm^3/g. As can be seen, the particles in the powder are separated even in the agglomerates and have a regular faceted shape. A particle size distribution bar chart is shown in Fig. 1b and the average particle size was 55 nm.

X-ray phase analysis (Fig. 1c) showed that the nanopowder content was 100% ScF_3. The calculated lattice parameter for ScF_3 did not differ significantly from the tabulated values[20] with $a = 0.40106$ nm.

Al-Based Metal Matrix Composite with ScF_3 Nanoparticles

The analysis of the latest literature data indicated that distribution of particles of different sizes in the matrix material in the process of solidification is also different.[21,22] The authors of Ref. 23 report that coarse particles (larger than 1 μm) are
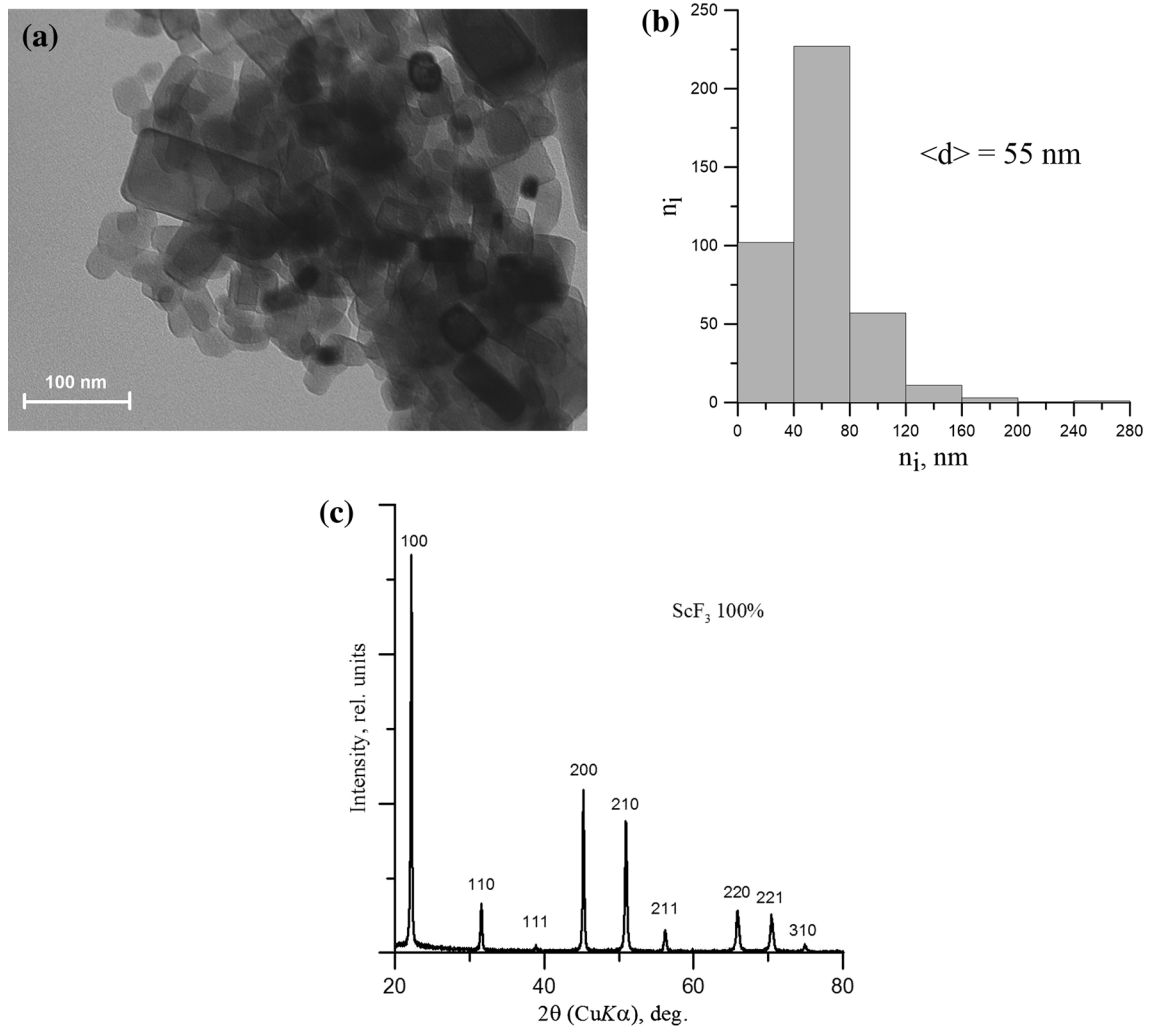
Fig. 1. TEM image of ScF$_3$ nanopowder (a), particle size distribution (b) and XRD pattern of ScF$_3$ nanopowder (c).

predominantly located in the grain body while nanoparticles are located along the grain boundaries. It can be assumed that the distribution of the particles in the ingot is determined by the solidification process. When alloys containing suspended particles cool, the interaction between the solidification front and the particles can be divided into two types: the particles are either absorbed by the front and therefore are distributed inside the grain, or the particles are "pushed" by the interface and end up in at the grain boundaries and eutectic areas.

SEM images of microstructure of the produced alloys are shown in Fig. 2. The structure of the alloys containing the ScF$_3$ nanoparticles does not differ significantly from the base alloy. Silicon inclusions were observed in the composites as in case of reference A356 alloy (Fig. 2a and b). Closer inspection of the structure, however, reveals ScF$_3$ nanoparticle clusters around silicon inclusions (Fig. 2c and d). The conclusion that the observed features of the structure represent clusters of ScF$_3$ nanoparticles is based on x-ray fluorescence analysis. The average distance between the clusters was

estimated as 3 μm. In this case, nanoparticle clusters were predominantly formed along the grain boundaries. The observed pattern of particle distribution in the alloy structure can be associated with attractive forces between nanoparticles as well as the influence of the solidification front.

The physics of flow stress (elastic limit) formation in composites is significantly more sophisticated than in monocrystalline and polycrystalline alloys. First, contributions of different strengthening mechanisms are not always additive. Secondly, in the process of plastic deformation, there are many substructural and phase transitions which change values and dependence of contributions on structural parameters. Thirdly, local stress concentrators are formed or material softening takes place in certain areas of the material. These factors lead to deformation localization, which makes it difficult to obtain stress estimates. Therefore, in each particular case, a detailed study of material is necessary in order to find the contribution of each of the mechanisms or a separate mechanism to the process of deformation that determines material's mechanical
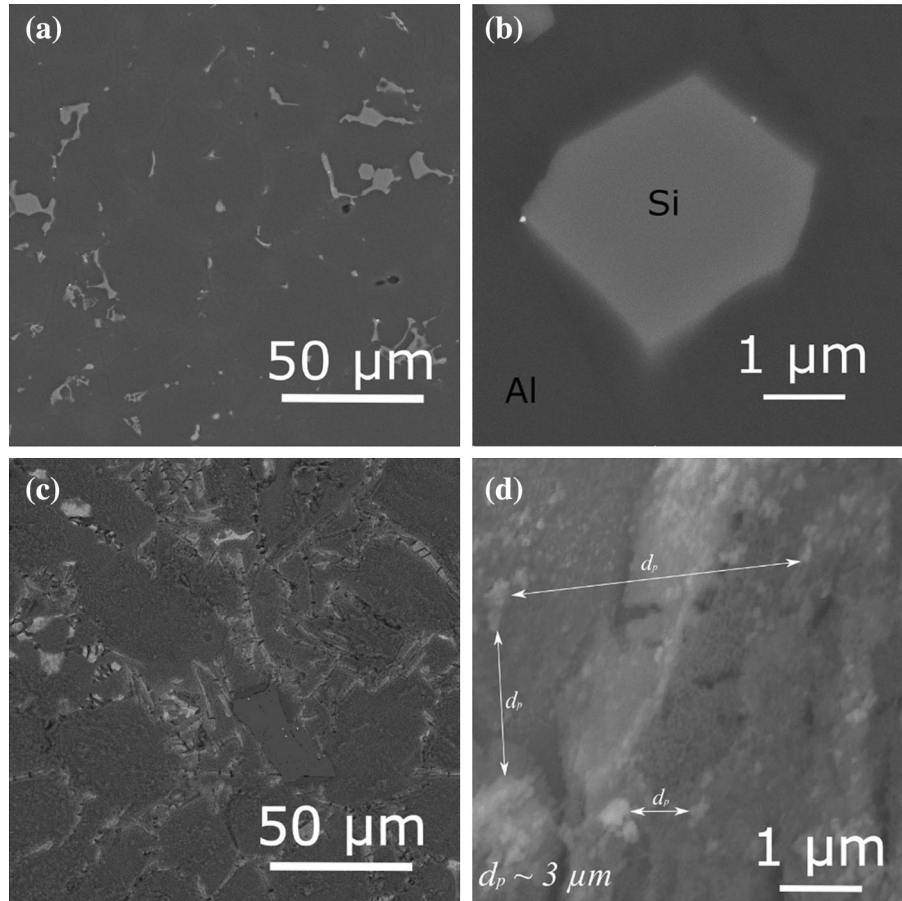
Fig. 2. SEM image of microstructure of the reference alloy (a, b) and A356 + 1 wt.% ScF_3 (c, d).

properties. In this respect, the influence of structural parameters of obtained alloys on their mechanical properties was studied.

Figure 3 shows the microstructure of the reference processed A356 alloy (a), processed MMC A356 + 0.2 wt.% ScF_3 (b) and processed MMC A356 + 1 wt.% ScF_3 (c). Figure 3d shows the microstructure of the unprocessed A356 alloy (without ultrasonic treatment or introduced nanoparticles). The average grain size in the reference alloy is 310 μm, and the introduction 0.2 wt.% of nanoparticles leads to the grain size reduction to 190 μm, while the introduction of 1 wt.% of nanoparticles reduces the grain size to 100 μm. Thus, the nanoparticles contribute to the significant (up to 3 times) reduction of the average grain size in the alloy.

The stress–strain tensile curves for the produced samples are given in Fig. 4. As can be seen, at similar values of yield strength, the introduction of 0.2% and 1% ScF_3 nanoparticles into the alloy leads to an increase of strain hardening coefficient (Fig. 4) compared with the unprocessed alloy. Moreover, alloy hardness also increases from 63 to 72 HV (Table I).

Improvement of the strength characteristics of heterogeneous systems in comparison with the homogeneous alloy can be associated with the presence of structural inhomogeneities and their properties. To estimate the contribution of various strengthening mechanisms to the mechanical behavior of obtained composites, let us consider the mechanics of the A356–ScF_3 system.

Load Bearing Strengthening

This strengthening mechanism explains a direct strengthening contribution from the reinforcement particles.[24] V_p is the volume fraction of ScF_3 calculated by Eq. 1:

$$V_p = 0.5 \frac{\text{wt.\%}/d_p}{(\text{wt.\%}d_p) + [(100 - \text{wt.\%})/d_m]} \times 100\%, \quad (1)$$

where d_p and d_m are the densities of ScF_3 (2.53 g/cm^3) and Al (2.7 g/cm^3), respectively. In the case of reinforcement particles bonded with a matrix

$$\sigma_{\text{load}} = 0.5 V_p \sigma_m \quad (2)$$

where σ_m is the yield strength of matrix alloy (80 MPa). σ_{load} was calculated to be ~0.35 MPa, which demonstrates a negligible change in the strength due to the load bearing of the reinforcement.
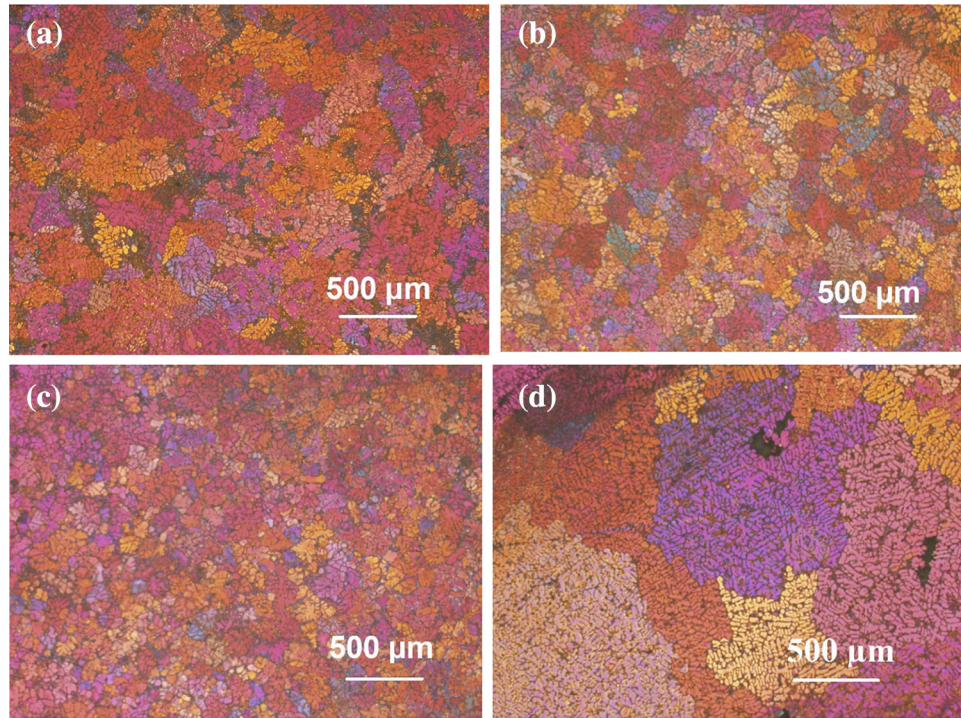
The Influence of ScF$_3$ Nanoparticles on the Physical and Mechanical Properties of New Metal
Matrix Composites Based on A356 Aluminum Alloy

3105

Fig. 3. The microstructure of (a) the processed reference A356 aluminum alloy and (b) MMCs: A356 + 0.2 wt.% ScF$_3$ and (c) A356 + 1 wt.% ScF$_3$. (d) The microstructure of the unprocessed alloy (without ultrasonic treatment and nanoparticles introduced).
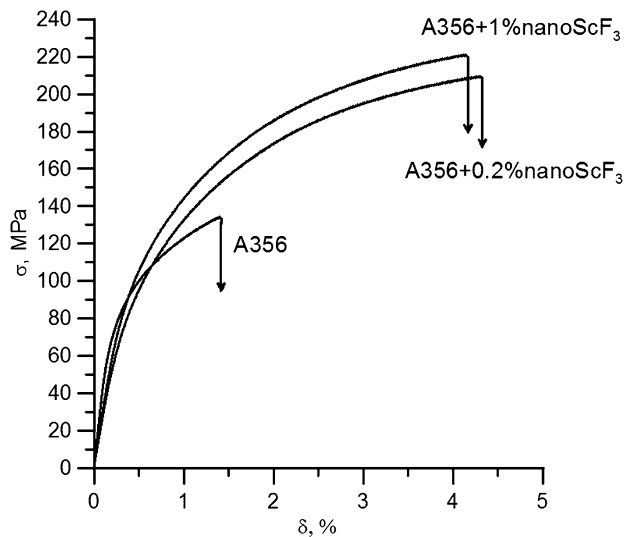

Fig. 4. The stress–strain tensile curves for produced samples of MMC.

Grain Refinement Strengthening

There are empirical models available for predicting the yield stress change due to the change in the grain size in MMCs by extending the Hall–Petch[24] relationship as follows:

$$\Delta\sigma_{GR} = k_y\left(D^{-1/2} - D_0^{1/2}\right) \qquad (3)$$

where D and D_0 are the average grain sizes of the obtained alloys given in Fig. 3a, b, and c and for the unprocessed alloy in Fig. 3d. This equation assumes that the Hall–Petch parameters K_y ($\sim$68 MPa $(\mu m)^{1/2}$ for Al alloys[25]) and σ_0 remain unchanged in the composites during processing. Taking into account the assessment of the average grain size (Fig. 3) $\Delta\sigma_{GR}$ values were calculated using Eq. 3. It was found that for the reference alloy $\Delta\sigma_{GR} \sim 2.5$ MPa, as for alloys with 0.2% of ScF$_3$ nanoparticles $\Delta\sigma_{GR} \sim 3.2$ MPa. Due to significant grain size reduction in alloys with 1% of ScF$_3$ nanoparticles, the value of $\Delta\sigma_{GR}$ was 3.7 MPa. Even though appreciable grain refinement was observed, the influence of grain refinement strengthening was estimated to be small. So it is worth looking for the influence of CTE mismatch strengthening.

Coefficient of Thermal Expansion (CTE) Mismatch Strengthening

When MMC is cooled from the processing temperature to room temperature, volumetric strain mismatch between matrix and reinforcement particles may occur due to the difference in CTE, which subsequently produces geometrically necessary dislocations around the reinforcement particles to accommodate the CTE difference.[26] When the length of the generated dislocation loop is assumed as πd_p, the strength increment from CTE strengthening can be estimated by

Table I. Mechanical properties of A356 based materials

Alloy	Hardness (HV)	Yield strength (MPa)	Tensile strength (MPa)	Elongation (%)
A356 reference	63 ± 2	85 ± 5	130 ± 15	1.4 ± 0.2
A356 + 0.2% ScF_3	65 ± 2	80 ± 15	195 ± 20	4.2 ± 1
A356 + 1% ScF_3	72 ± 3	90 ± 10	215 ± 10	4 ± 0.8

$$\Delta\sigma_{CTE} = \beta G b \left[\frac{12(\alpha_m - \alpha_p)\Delta T V_p}{b d_p (1 - V_p)} \right]^{1/2} \quad (4)$$

where β is a constant ~ 1.25, α_m is the CTE of the aluminum matrix (23×10^{-6}/K) and α_p is the CTE of the particles (-8×10^{-6}/K). ΔT is the difference between the processing temperature (725°C) and room temperature (25°C). d_p is taken as the average distance between the clusters ($\sim 3~\mu$m), and the shear modulus is estimated by:

$$G = \frac{0.5 E_m}{1 + \vartheta} \quad (5)$$

where E_m is Young's modulus of matrix alloy, 70 GPa, K is Poisson's ratio, 0.33, and b is the Burgers vector (0.286 nm). Therefore, $\Delta\sigma_{CTE}$ was estimated to be ~ 20 MPa for the alloy with 1% of ScF_3 nanoparticles. This showed that the CTE mismatch can be a dominant strengthening mechanism in the composites obtained in the present study.

CONCLUDING REMARKS

It has been found that, in the process of solidification of an A356 alloy, ScF_3 nanoparticles clusters are formed which affect the properties of the composites. The introduction of is preformed mixture containing ScF_3 nanoparticles into the aluminum melt with simultaneous ultrasonic treatment leads to the decrease in the grain size of up to three times. Moreover, the introduction of ScF_3 nanoparticles into the alloy leads to improvements in the ultimate tensile strength and ductility of the resultant MMC. Alloy hardness also increases from 63 HV to 72 HV. Apparently, the contribution to the increase of is mechanical properties of the materials comes from the grain boundary and particulate strengthening mechanisms. However, the CTE mismatch strengthening mechanism makes the most significant contribution to the strengthening of is composite structure due to is negative coefficient of thermal expansion of ScF_3.

ACKNOWLEDGEMENT

REFERENCES

1. S. Vorozhtsov, V. Kolarik, V. Promakhov, I. Zhukov, A. Vorozhtsov, and V. Kuchenreuther-Hummel, *JOM* 68, 1312 (2016).
2. S. Vorozhtsov, D. Eskin, A. Vorozhtsov, and S. Kulkov, *Light metals 2014*, ed. J. Grandfield (Warrendale, PA: TMS, 2014), pp. 1373–1377.
3. S.A. Vorozhtsov, D.G. Eskin, J. Tamayo, A.B. Vorozhtsov, V.V. Promakhov, A.A. Averin, and A.P. Khrustalyov, *Metall. Mater. Trans. A* 46A, 2870 (2015).
4. M. Tabandeh-Khorshid, E. Omrani, P.L. Menezes, and P.K. Rohatgi, *Eng. Sci. Tech. Int. J.* 19, 463 (2016).
5. A. Mazahery, and M.O. Shabani, *JOM* 2, 323 (2012).
6. S.P. Dwivedi, S. Sharma, and R. Kumar Mishra, *Adv. Mat. Manuf. Char.* 14, 81 (2014).
7. T. Zienert and O. Fabrichnaya, *Edv. Eng. Mat.* 15, 1244 (2013).
8. S.A. Vorozhtsov, A.P. Khrustalyov, D.G. Eskin, S.N. Kulkov, and N. Alba-Baena, *Rus. Phys. J.* 57, 1485 (2015).
9. A.A. Gromov, S.A. Vorozhtsov, V.F. Komarov, G.V. Sakovich, YuI Pautova, and M. Offermann, *Mater. Lett.* 91, 198 (2013).
10. S. Vorozhtsov, I. Zhukov, A. Vorozhtsov, A. Zhukov, D. Eskin, and A. Kvetinskaya, *Adv. Mater. Sci. Eng.* 2015, 1 (2015).
11. H. Choi and X. Li, *J. Mater. Sci.* 47, 3096 (2012).
12. S. Candan, *Mater. Lett.* 58, 3601 (2004).
13. D.P. Mondal, N.V. Ganesh, V.S. Muneshwar, S. Das, and N. Ramakrishnan, *Mater. Sci. Eng. A* 433, 18 (2006).
14. Ch. Weng Wong, M. Gupta, and L. Lu, *J. Mater. Sci.* 34, 1681 (1999).
15. L.P. Soon and M. Gupta, *J. Mat. Sci. Lett.* 20, 323 (2001).
16. T.S. Srivatsan, *J. Mat. Sci.* 31, 1375 (1996).
17. O. Kudryashova and S. Vorozhtsov, *JOM* 68, 1307 (2016).
18. G.I. Eskin and D.G. Eskin, *Ultrason. Sonochem* 10, 297 (2003).
19. C.J. Brinker and G.W. Scherer, *Sol-gel science* (Academic Press, 1990), p. 881.
20. B.K. Greve, K.L. Martin, P.L. Lee, P.J. Chupas, and K.W. Chapman, *J. Am. Chem. Soc.* 132, 15496 (2010).
21. L.Y. Chen, J.Y. Peng, J.Q. Xu, H. Choi, and X.C. Li, *Scr. Mater.* 69, 634 (2013).
22. H. Ferkel and B.L. Mordike, *Mater. Sci. Eng. A* 298, 193 (2016).
23. X.H. Chen and H. Yan, *Mater. Des.* 94, 148 (2016).
24. N. Ramakrishnan, *Acta Mater.* 44, 69 (1996).
25. G. Neite, K. Kubota, K. Higashi, and F. Hehmann, *Mater. Sci. Tech.* 8, 115 (2005).
26. V.M. Sreekumar, N.H. Babu, D.G. Eskin, and Z. Fan, *Mater. Sci. Eng. A* 628, 30 (2015).